# MODELING OF AN ATMOSPHERIC-BOUNDARY-LAYER PROFILE IN SUPPORT OF EXPERIMENTS IN THE NASA LANGLEY TRANSONIC DYNAMICS TUNNEL

**Pawel Chwalowski and Thomas G. Ivanco**[1]

[1]Aeroelasticity Branch, NASA Langley Research Center, Hampton, VA 23681, USA
Pawel.Chwalowski@nasa.gov

**Keywords:** Unsteady Aerodynamics, CFD, MDDES, FUN3D, TDT, ABL.

**Abstract:** This paper presents the results of the Computational Fluid Dynamics (CFD) analyses to model two atmospheric-boundary-layer (ABL) profiles inside the NASA Langley Research Center Transonic Dynamics Tunnel (TDT). The CFD models include tunnel walls and all additional hardware needed to simulate the ABL profiles. This hardware includes Irwin spires and floor-mounted roughness elements. The numerical simulations show that the application of higher-fidelity numerical methods is necessary to compute boundary-layer and turbulence-intensity profiles that match experimental data. The ABL profiles are computed both inside the numerical model of the TDT and in a classical free-air model. Both Unsteady Reynolds-Averaged Navier-Stokes (URANS) with Spalart-Allmaras (SA) turbulence model and Modified Delayed Detached Eddy (MDDES) simulation methods are used. The results show that the MDDES-simulation results match the experimental data very well while URANS-SA does not. The results also show that the wind-tunnel walls have a significant effect on ABL prediction.

## 1 INTRODUCTION

The Transonic Dynamics Tunnel (TDT), located at the NASA Langley Research Center, is a continuous-flow, closed circuit, variable pressure wind tunnel, with a 16- by 16-foot slotted test section with cropped corners. It has the capability to use either air or R-134a heavy gas as a test medium. In this study, experimental data acquired in the R-134a test medium was compared with the computational data. TDT's unique capabilities are well described and summarized in the publication by Ivanco [1], where he states the following: "Typically regarded as the world's premier aeroelastic test facility, TDT fulfills a unique niche in the wind tunnel infrastructure as a result of its unparalleled ability to manipulate fluid-structure scaling parameters." A sketch and plan view of the TDT are shown in Figures 1a and 1b, respectively.

The development of a Computational Fluid Dynamics (CFD) model of the TDT allows for realistic comparisons of the experimental data collected in the tunnel with computational data. By including the tunnel walls in the computational model, for example, the uncertainty associated with the tunnel wall interference effects is significantly reduced. The validation of the CFD model of the TDT in 2012 used experimental data obtained during empty tunnel calibration [2]. The fundamental parameters matched between the experiments and computations included boundary-layer profiles, wall pressures, and centerline Mach number at various flow conditions.

Since its initial validation, the TDT CFD model has been used to predict a flutter event that occurred during testing of a generic fighter flutter experiment [3, 4]. During this experiment,

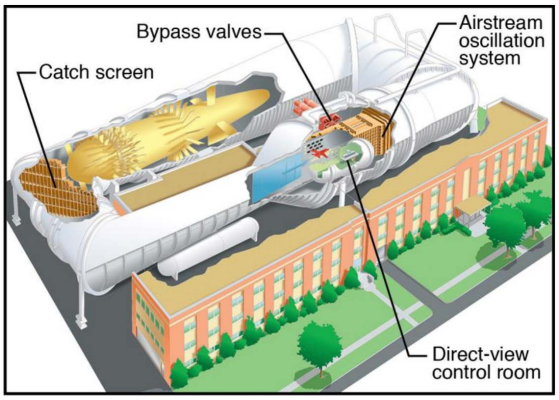


(a) Sketch of the Transonic Dynamics Tunnel with cutaways showing key features.

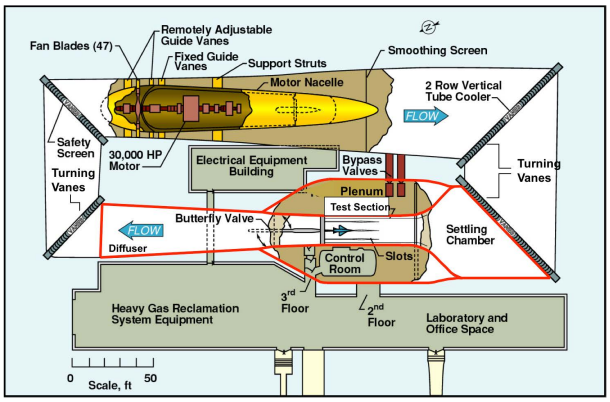


(b) Plan view of the Transonic Dynamics Tunnel with red lines showing the computational domain.

Figure 1: Transonic Dynamics Tunnel sketch and plan view.

flutter occurred, damaging wings of the test article. This flutter event was computed, assuming first a free-air model and then a model including the wind-tunnel walls. The assessment from that study was that the wind-tunnel walls did not affect the response of the aircraft model and that the flutter prediction for both computational models was essentially the same [5].

This numerical study supplements a recently completed experimental test campaign in the TDT. The purpose of these experiments was to develop representative atmospheric boundary layer (ABL) profiles for three different launch pad sites [6]. An ABL, which includes both an average wind profile and turbulence content, is one of the aerodynamic characteristics affecting the occurrence of wind-induced oscillations of a launch vehicle sitting on a launch pad. The primary purpose of this paper is to determine if the CFD software is capable of predicting an ABL profile. The secondary purpose is to demonstrate that tunnel walls *do* have an effect on the experimental data. With that in mind, the computational models were constructed both with and without tunnel walls to quantify the tunnel-wall effect on the prediction of the ABL.

## 2 ABL-PRODUCING HARDWARE USED IN THE TDT

In the TDT ABL experiments, Irwin spires [7] were installed at the entrance to the test section in the region of the converging nozzle. This allowed for an approximate 42-foot distance, called the fetch length, for the flow to develop the desired characteristics and the velocity profile shape to simulate an ABL prior to impacting a launch vehicle model that would be mounted on the TDT's floor turntable. In addition, floor-mounted roughness elements, either 3-inch or 6-inch wooden cubes, were installed in various configurations along the fetch length to help sustain the spire-induced turbulence and to alter the boundary-layer profile. A photograph of one of the tested spire-and-block configurations is presented in Figure 2. The pictures in Figures 3a and 3b depict an example of the size and location of the spires and cubes. Note that the measurement of the ABL profile in the TDT is at the location denoted as TS 72 in Figure 3b. This refers to the tunnel station 72 feet that is located at the center of the turntable as shown in Figures 3a and 3b. This is the mounting location for the launch vehicle associated with this work. While several spire-plus-cube configurations were tested in the TDT, the corresponding CFD study was only done for two configurations: one attempting to match the average ABL at the Cape Canaveral Air Force Station Space Launch Complex 40 (SLC-40) and the other attempting to match ABL at the Kennedy Space Center Launch Complex 39b (SLC-39), both in Florida. The difference between the two wind-tunnel ABL configurations is that the SLC-40 includes both

spires and cubes, while SLC-39 consists of spires only. The top view schematic of the SLC-40 spire-and-cube configuration is shown in Figure 4.

Data for ABL characterization was acquired with an instrumented flow survey rake positioned in the tunnel such that measurements were obtained at approximately TS 72, which corresponded to the center of the floor turntable where the launch vehicle models would be located [6]. The rake is identified in Figure 2. Instruments were distributed along the 12-foot long rake in one-foot increments and consisted of four steady pitot-static pressure probes, two unsteady total pressure probes, two unsteady static pressure probes, two unsteady five-hole probes, and a total temperature probe. The unsteady five-hole probes were used to derive a time history of velocity in all three axes.

The instrumented rake was mounted on a traversing and rolling sting. During testing, tunnel conditions were held constant while the rake was traversed vertically and rotated to various angles in order to map the flow volume. The rake was also inverted so that complementary instruments, such as steady versus unsteady, could attain measurements at the same flow position. Measurements were taken in vertical increments of one foot and were obtained as close to the test section ceiling and turntable face as the sting support system would safely allow, approximately eight and six inches, respectively. Rotation angles were chosen so that probes were translated laterally to replicate measurements taken in the vicinity of the test section centerline by steady probes with the complementary unsteady probes in addition to the five-hole probes.

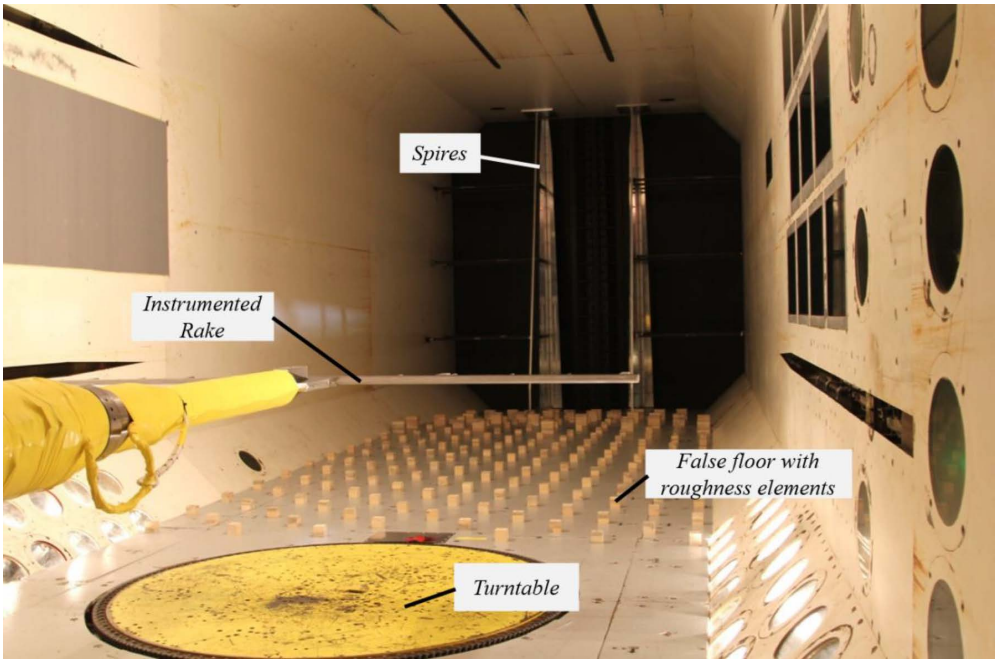


Figure 2: Photo of a sample configuration of spire and roughness elements (blocks) installed in the TDT, with instrumentation flow survey rake in the foreground, looking upstream.

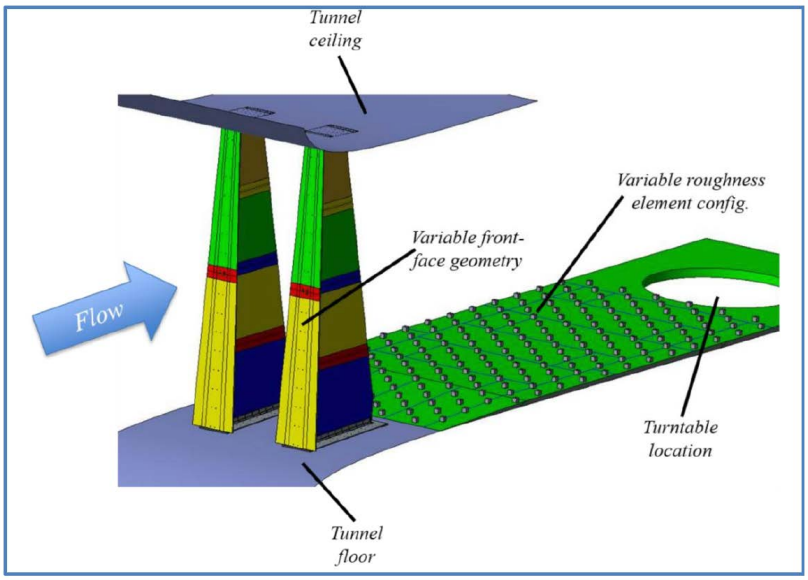


(a) Irwin spire shape and roughness elements (blocks).

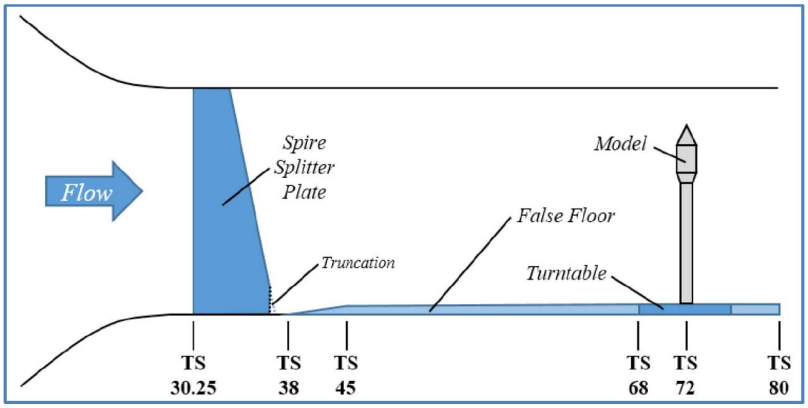


(b) Location of spires in TDT.

Figure 3: Modification to TDT for ABL profile measurement.

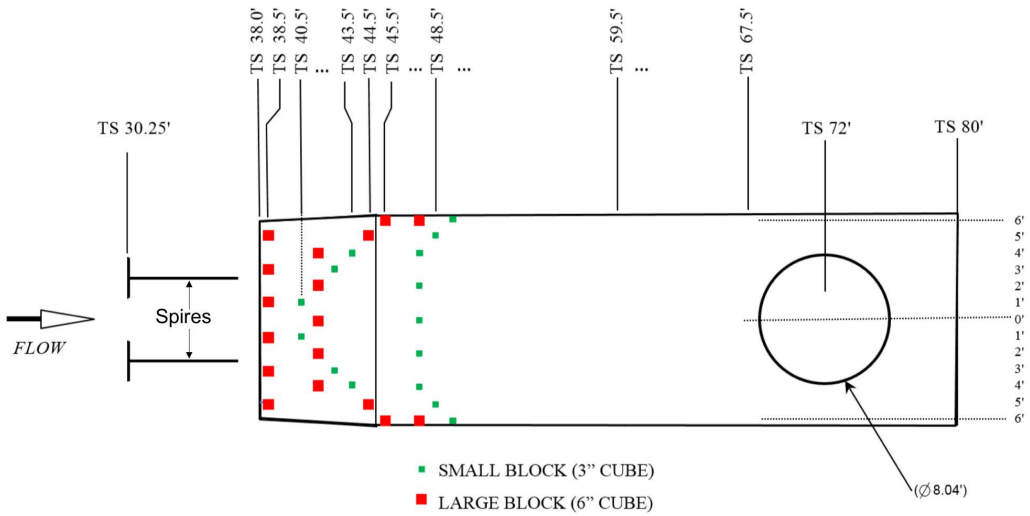


Figure 4: Top view of SLC-40 spire locations and roughness block distribution with key features of the test section, tunnel station in feet.

## 3 COMPUTATIONAL DOMAIN AND MESH

In the TDT plan view shown in Figure 1b, the red line around the test section of the tunnel defines the outline of the computational domain used in the CFD analysis. The domain begins with the settling chamber and continues into the test section leg, where it is connected with the plenum via slots in all four walls and a system of reentry flaps. The domain ends at the exit plane of the diffuser. The shape of the computational domain at the settling chamber is not desirable for the numerical analysis because of the corners where the walls of the chamber meet the turning vanes. However, to include the turning vanes in the computational model together with the rest of the tunnel geometry is too computationally expensive at this time. Therefore, the vanes were excluded from the CFD model.

This study utilizes an 'as-built' surface geometry of the TDT as opposed to 'per-drawing' or the idealized geometry provided in the drawing plans. The same approach was used by Nayani [8] in his analysis of the NASA Langley Research Center 14- by 22-Foot Subsonic Tunnel. To obtain 'as-built' geometry for both tunnels, laser scans of the desired regions were conducted. For the TDT test section, the laser scan produced a point cloud database of approximately 15.5 million points through which surfaces were fitted in preparation for grid generation. The details of the surface-fitting process can be found in reference [2].

Unstructured tetrahedral grids were used in this study. They were generated using VGRID [9] with input prepared using GridTool [10]. The tetrahedral elements within the boundary layer were converted into prism elements using preprocessing options within the NASA Langley FUN3D software [11]. First-cell height away from the wall was set to $9 \times 10^{-6}$ feet, which ensured the average $y^+ < 1$. For each case considered in this study, (1) empty tunnel, (2) tunnel with spires, and (3) tunnel with spires and blocks, two meshes with consistent size and resolution were used, which for simplicity, are labeled as 'Mesh A' and 'Mesh B' in this paper. Mesh A is considered a coarse mesh and for the SLC-40 configuration consists of about 89 million nodes. Mesh B for SLC-40 configuration was constructed in two steps. First, a global refinement was done on Mesh A, which resulted in a 109 million node mesh. Then, a local refinement was performed between the spires and TS 72 that resulted in a 130 million node mesh.

Figure 5 shows the outside surface mesh of the TDT computational domain using Mesh B. Figure 6a depicts the ABL hardware setup inside the TDT test section. Figure 6b shows a close-up view of the region and surface mesh inside the tunnel as depicted in Figure 6a. Figures 6c and 6d show the mesh distribution at the TS 72 cross section for Mesh A and Mesh B, respectively. Note that the instrumented rake described earlier was not included in the computational model.

## 4 COMPUTATIONAL APPROACH

### 4.1 Flow Solver

FUN3D software [11], which was developed at the NASA Langley Research Center, was used in this analysis. FUN3D is a finite-volume, unstructured-grid, node-based, mixed-element Unsteady Reynolds Averaged Navier-Stokes (URANS) flow solver. Various turbulence models are available. The flow condition of interest for this study was Mach 0.25 so the flux limitation was not needed. Inviscid fluxes were computed using the Roe flux-difference splitting scheme [12]. For the asymptotically-steady cases under consideration, time integration was accomplished by

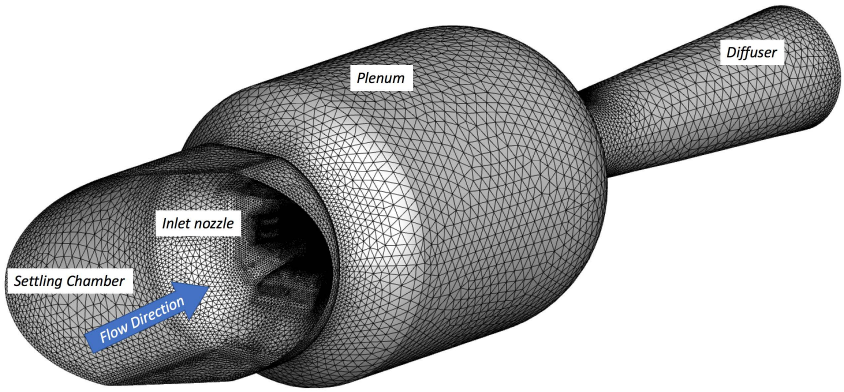


Figure 5: TDT computational mesh example; an outside view, Mesh B.

an Euler implicit backwards difference scheme, with local time stepping to accelerate convergence. The unsteady results were computed and compared using Spalart-Allmaras (SA) [13] turbulence model and Modified Delayed Detached Eddy Simulation (MDDES) [14]. The advancement in time for unsteady computations was accomplished using a second-order backward difference scheme [15].

### 4.2 Boundary Conditions

For this study, a total pressure and total temperature boundary condition was used at the settling chamber. The shape of the computational domain at the inlet requires specification of the inlet flow angle at the plane where the turning vanes are located (see Figure 1b). This angle was measured to be 38°. At the exit of the diffuser, a back pressure boundary condition was used. Back pressure is not a measured quantity in the TDT, so the value was iterated to achieve the desired Mach number in the test section. The desired Mach number is determined based on the computed static pressure in the plenum and the total pressure at the inlet. Every computation was run 'from scratch' whenever the back pressure was changed. This procedure was adopted when it was observed that restarting a solution from the previous solution, after changing the back pressure, resulted in oscillations in the flow field requiring many iterations to damp out.

### 4.3 Solution Process

The first step in the solution process was to initialize the flow to total pressure and total temperature in the settling chamber and to the static pressure elsewhere. The steady-state solution was then obtained. The steady-state cases in this study were run for about 7,000 iterations to achieve an approximate seven order-of-magnitude drop in residuals. Each steady-state computation using Mesh B took approximately 6 hours on 784 Broadwell cores on the NASA Advanced Supercomputing (NAS) Pleiades supercomputer. The unsteady solutions were always restarted from the steady-state solution.

In a typical unsteady computation, the time-step size is chosen based on the fraction of the time it takes a fluid particle to travel a characteristic distance. For example, in the case of the airplane simulation, a mean aerodynamic chord is usually chosen as a characteristic distance. In this study, we chose frequencies of interest, between 6Hz and 190Hz, as a guide to compute the time-step size. Based on the 190 Hz frequency and the 1/200 fraction, the physical time-step size is about $2.6 \times 10^{-5}$ seconds. This time-step size is labeled as Time 3. Two additional time-step sizes were also considered: five times (Time 2) and 25 times (Time 1) larger than the Time

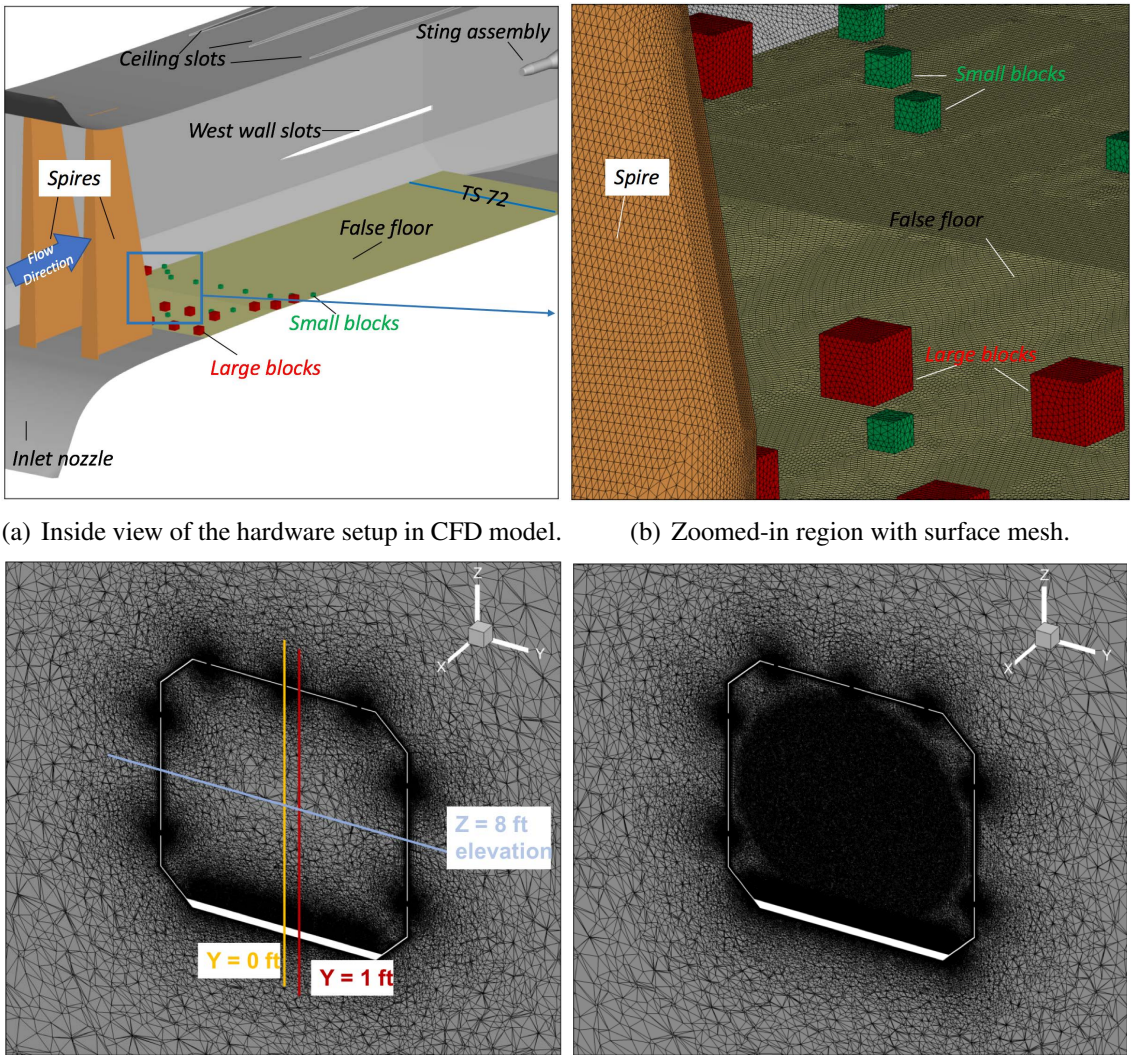


(a) Inside view of the hardware setup in CFD model.

(b) Zoomed-in region with surface mesh.

(c) Cross section of Mesh A at TS 72.

(d) Cross section of Mesh B at TS 72.

Figure 6: Hardware setup and computational mesh for the SLC-40 configuration.

3 time-step size. The unsteady computations were first restarted from the steady-state solution using the largest time-step size and the flow solver was run for about 15,000 time steps. Then, the computation was restarted with an intermediate time-step size and the flow solver was run for another 15,000 time steps. Finally, the smallest time-step size, Time 3, was used to obtain the solution. This process allowed the time-averaged quantities to be obtained from each individual phase of the solution. The computational results with the Time 1 and Time 2 time-step sizes are essentially the same, and therefore, all the results shown below were obtained with the Time 2 time-step size only. The results obtained with Time 3 are considered preliminary, because not enough data time record was obtained for averaging purposes. The first phase of the unsteady computation using Mesh B and Time 1 took approximately 15 days on 784 Broadwell cores on the Pleiades supercomputer.

## 5 RESULTS

The ABL consists of two quantities: the boundary-layer profile and the velocity turbulence intensity profile. The computed and experimental boundary-layer profiles presented here are plotted as the mean velocity normalized by the reference velocity as a function of tunnel elevation at the lateral center of the tunnel, Y = 0 ft and at TS 72. The reference velocity is

the velocity at an elevation of eight feet. The velocity turbulence intensity is computed as the standard deviation of velocity as a function of tunnel elevation at a lateral location of Y = 1 ft (location of the unsteady total pressure probe on the rake) and normalized by the local mean velocity.

The computed ABL profiles for the SLC-40 configuration are shown in Figure 7. The results include (1) MDDES computations on both Mesh A and Mesh B for the SLC-40 configuration, (2) the MDDES computation assuming an empty tunnel without spires and blocks (as a reference), (3) the URANS-SA computation on Mesh B only, and (4) the experimental data. While it appears in Figure 7a that the URANS-SA simulation produces a boundary-layer profile that closely matches the experimental data, further examination of these results is necessary. Figures 8 and 9 present the normalized mean velocity extended to Y= $\pm$ 1 and $\pm$ 2 feet lateral locations for the URANS-SA and MDDES solution on Mesh B, respectively. As seen in Figure 8a, the URANS-SA solution is characterized by a definite shift in lateral direction in boundary-layer profiles. This is in contrast with the MDDES solution, where the boundary-layer profiles, as presented in Figure 9a, stays more constant within the Y= $\pm$ 2 feet range. This is also visually represented by the corresponding normalized velocity surfaces at TS 72 shown in Figures 8b and 9b. The URANS-SA solution produces steady-state 'valleys' downstream of the spires due to lack of velocity fluctuations. The MDDES solution, on the other hand, computed these fluctuations, and the averaged velocity produces a uniform surface. The effects of the tunnel walls on the velocity distribution are also visible in these figures. In addition, the 'dents' in the velocity surface on top and sides represent flow through the tunnel's slots.

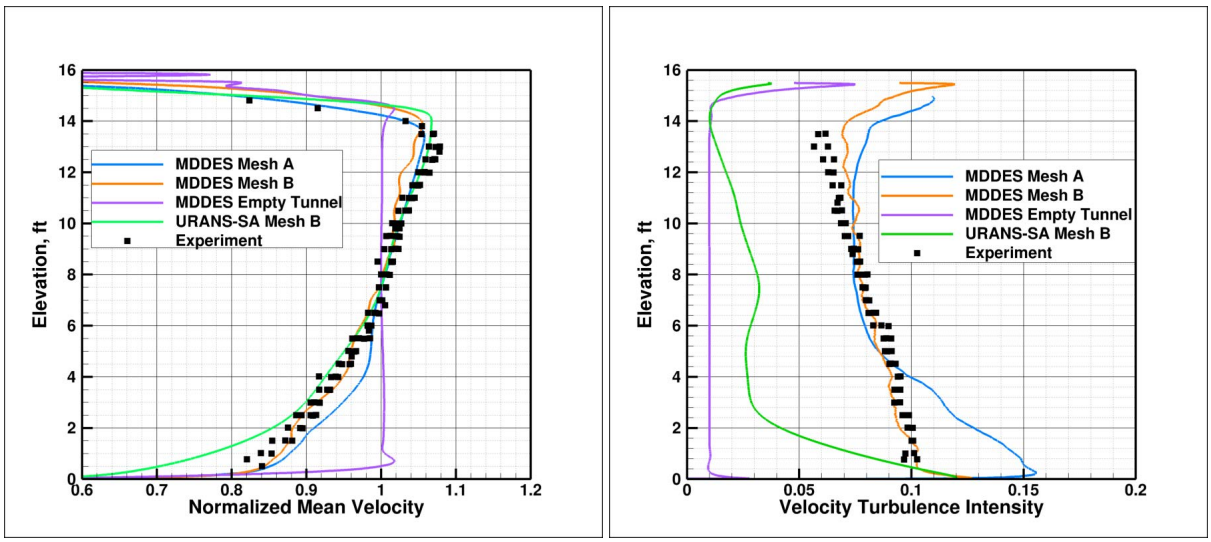


(a) Boundary-layer profile, Y = 0 ft. (b) Velocity turbulence intensity profile, Y = 1 ft.

Figure 7: Computed SLC-40 ABL profiles: URANS-SA and MDDES solutions, Mesh A and Mesh B, Time 2.

In addition, Figure 7 demonstrates the importance of proper mesh density in the MDDES simulations. The computations performed on Mesh B produced a much better agreement with both the experimental boundary-layer profile and the velocity turbulence intensity data than the computations on the less dense Mesh A. Figure 7 also presents the computed boundary-layer profile and the velocity turbulence intensity profile for an empty tunnel. Clearly, and as designed, the inclusion of the spires and blocks changes the velocity profile and turbulence intensity. It should be noted that the turbulence intensity computed using the URANS-SA method is closer to the empty-tunnel MDDES results than it is to the MDDES SLC-40 configuration results. This is because the URANS-SA solution lacks the velocity fluctuations and produces more of a steady-

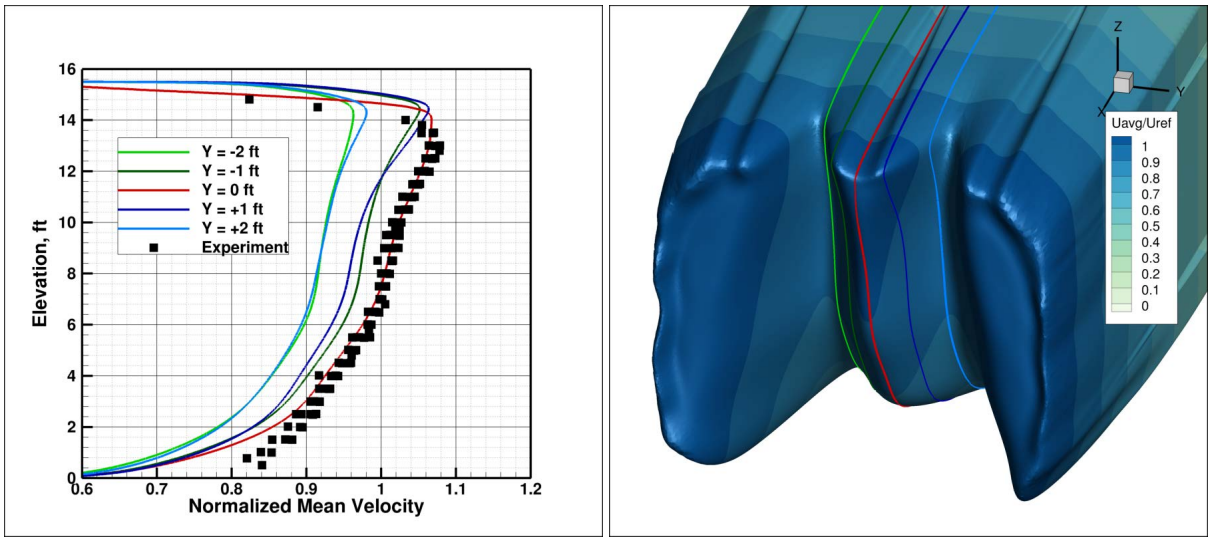


(a) Boundary-layer profile at Y = ±1, ±2, and 0 ft. (b) Surface of the normalized mean velocity.

Figure 8: Computed (URANS-SA, Mesh B, Time 2) normalized mean velocities near tunnel centerline at TS 72 compared to experimental data (Y = 0 ft), SLC-40.

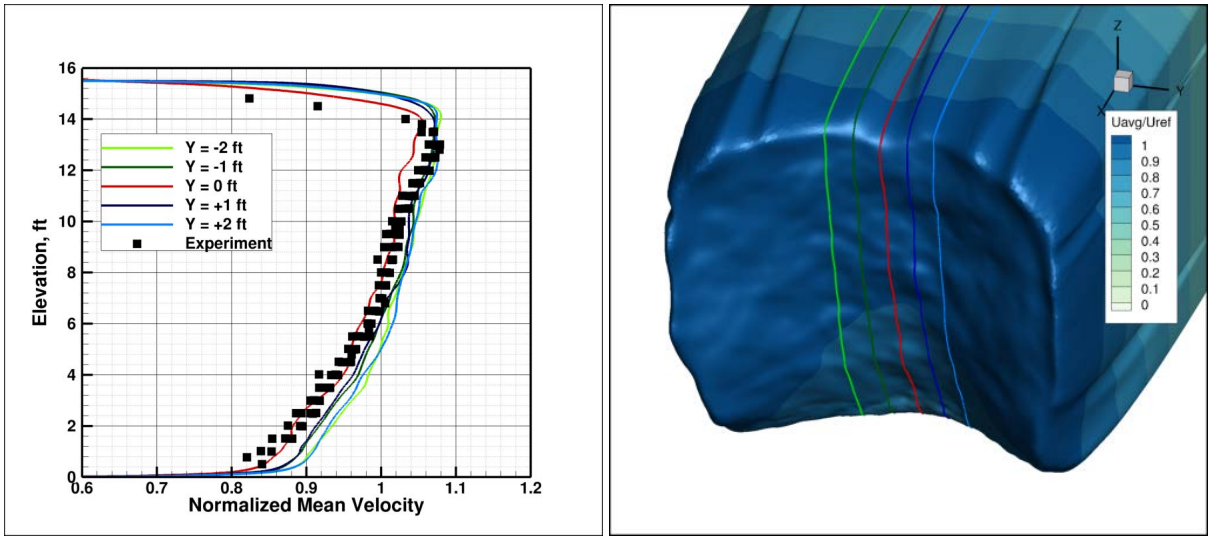


(a) Boundary-layer profile at Y = ±1, ±2, and 0 ft. (b) Surface of the normalized mean velocity.

Figure 9: Computed (MDDES, Mesh B, Time 2) normalized mean velocities near tunnel centerline at TS 72 compared to experimental data (Y = 0 ft), SLC-40.

state flow downstream of the spires. Although the empty tunnel results were obtained using only the MDDES method, it is assumed that the URANS-SA should produce similar profiles. Note that the experimental data in an empty tunnel in R-134a were not obtained during this test campaign, so they are not available for comparison.

The computed ABL profiles for the SLC-39 configuration are presented in Figure 10. This configuration used only the spires. Blocks were not present. For this simulation, only MDDES solutions on two meshes were obtained. Figure 10a shows the computed boundary-layer profiles and Figure 10b shows the computed velocity turbulence intensities. As was seen for the SLC-40 solution, the computation for SLC-39 using Mesh B produced better agreement with the experimental data than did the Mesh A computation.

The dimensional power spectral density (PSD) at Y = 1 ft and Z = 8 ft (see Figure 6c) computed

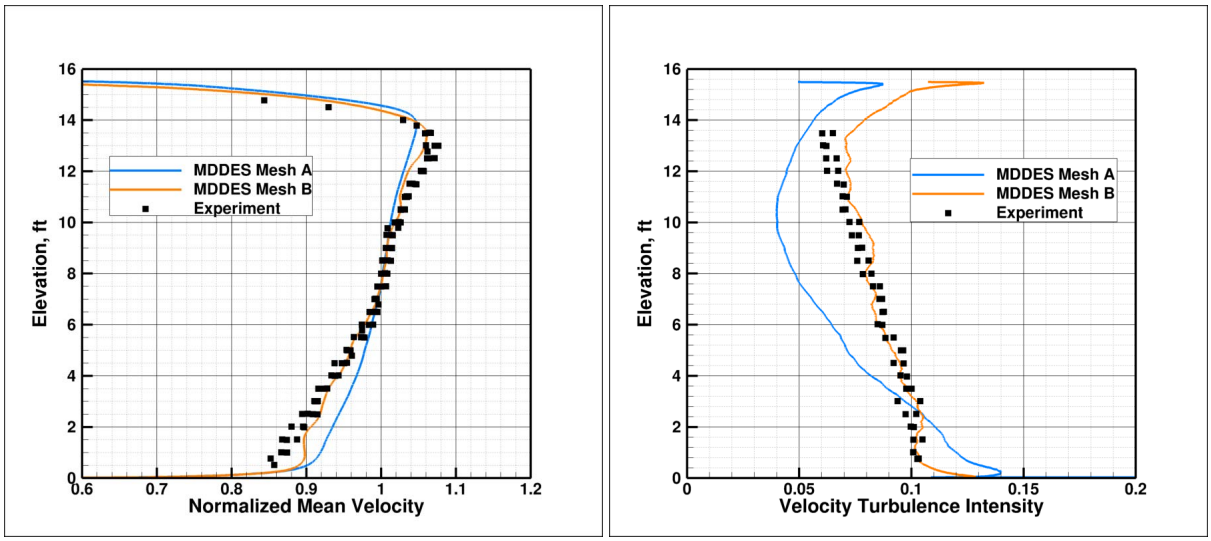


(a) Boundary-layer profile. (b) Velocity turbulence intensity.

Figure 10: Computed SLC-39 ABL profiles: MDDES solutions, Mesh A and Mesh B, Time 2.

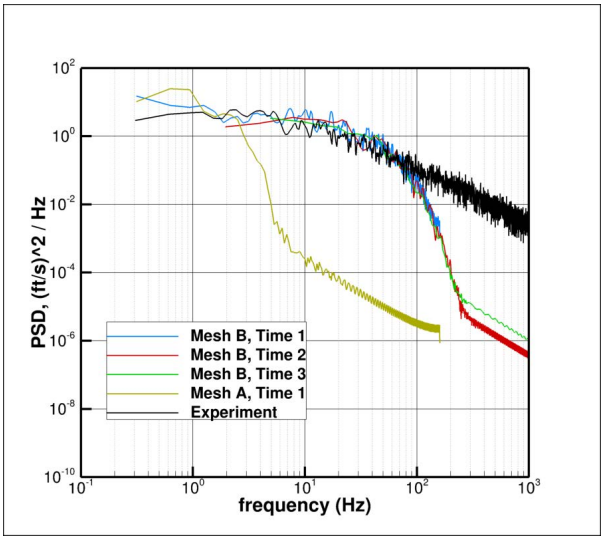


Figure 11: Dimensional turbulence spectra computed from measured TDT data at Y = 1 ft and compared with MDDES method using Mesh A and B, and Time 1, Time 2, Time 3.

from the TDT data and MDDES method is shown in Figure 11. The computational turbulence spectra obtained from the MDDES simulations using Mesh B and the three time-step sizes closely match the turbulence spectra from the wind-tunnel in the frequency range up to 90Hz. The spectra were computed using MATLAB's 'pwelch' function and a Hamming window with a 50% overlap and a default number of points [16]. The spectra seems to be more dependent on the mesh density (spatial resolution) than the time-step size (temporal resolution) used in the computations. For example, the solution using Mesh A only matches the experimental data at low frequencies. The turbulence spectra comparison suggests that further mesh refinement is necessary. On the other hand, it appears that the computed ABL profiles (see Figure 7b) are independent of the high frequency content in turbulence spectra.

## 6 FREE-AIR MODEL VS. TDT MODEL

A computational model of the SLC-40 configuration without the wind-tunnel walls, similar to the one shown in reference [17], was constructed to determine the effect of the walls on the ABL prediction. This model is shown in red in Figure 12a. To construct the free-air (FA) model, the wind-tunnel side walls were replaced with planes of symmetry, the wind-tunnel floor was kept as a viscous wall, and the domain was extended vertically. The free-stream boundary condition was applied at the inlet. In addition, the height of the spires was extruded up by about two feet to alleviate potential spire-tip effects on the boundary-layer profile. However, in future analyses the height of the spires will be increased further per recommendations in references [6] and [7]. The surface roughness block structure was the same as in the SLC-40 TDT-model configuration. Figure 12b shows the MDDES computed boundary-layer profiles for the FA model, the TDT model using Mesh A, and the experimental data. These results show that the wind-tunnel walls *do* have significant effect on the ABL prediction and cannot be ignored in computational models.

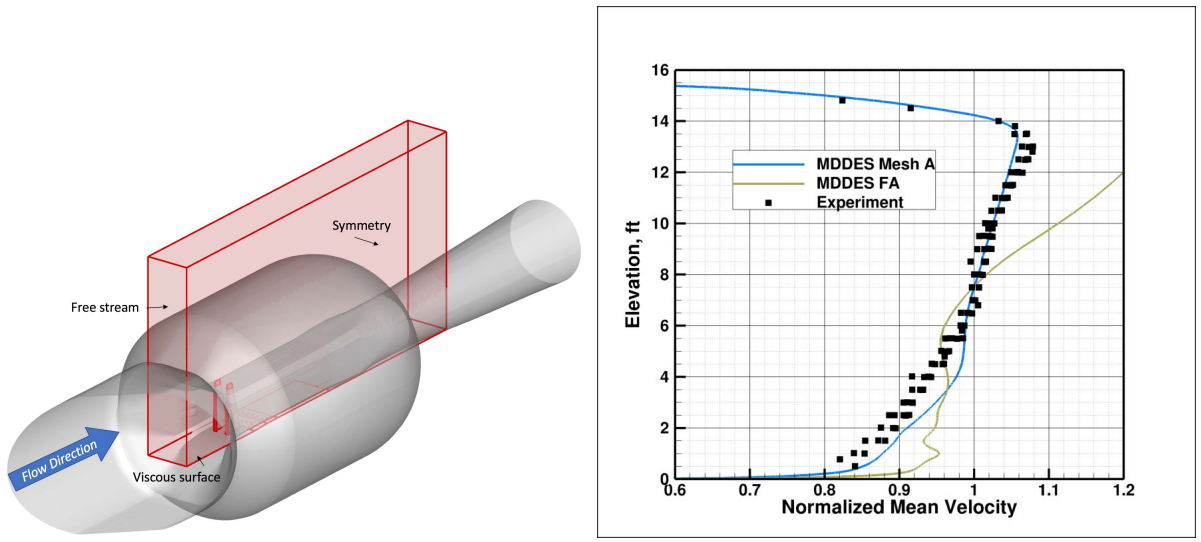


(a) Computational domain. (b) Boundary-layer profile.

Figure 12: Free-air computational model description and results.

## 7 CONCLUDING REMARKS

The first objective of this study was to compute the ABL profiles using the computational model of the TDT. The profiles were computed using both URANS-SA and MDDES solutions and were compared against the experimental data. The results demonstrate that the MDDES solution, using a higher density mesh, produced very good agreement with the experimental data for both the boundary-layer profile and the velocity turbulence intensity profile. The second objective was to compare the computational results obtained in the TDT model with those obtained in a classical free-air model. The results showed that the wind-tunnel walls *cannot* be ignored in the computational model. Future analysis will extend this work to examine temporal and spatial convergence and the necessary time-record length for velocity averaging.

## 8 ACKNOWLEDGMENTS

The computational analyses were conducted at the NASA Advanced Supercomputing Center located at NASA Ames Research Center. The authors would like to acknowledge help from several members of the Aeroelasticity Branch at NASA Langley Research Center: Dr. Jennifer Heeg, Dr. Kevin Jacobson, and Ms. Jennifer Pinkerton. In addition, the authors would like to acknowledge discussions with and help from Dr. Christopher Rumsey from the Computational Aerosciences Branch at NASA Langley Research Center.

## 9 REFERENCES

[1] Ivanco, T. G. (2013). Unique Testing Capabilities of the NASA Langley Transonic Dynamics Tunnel, an Exercise in Aeroelastic Scaling. AIAA Paper 2013-2625.

[2] Chwalowski, P., Quon, E., and Brynildsen, S. E. (2016). Computational Analysis of the Transonic Dynamics Tunnel. AIAA Paper 2016-1775.

[3] Silva, W. A., Ringertz, U., Stenfelt, G., et al. (2016). Status of the KTH-NASA Wind-Tunnel Test for Acquisition of Transonic Nonlinear Aeroelastic Data. AIAA Paper 2016-2050.

[4] Silva, W. A., Chwalowski, P., Wieseman, C. D., et al. (2017). Computational Results for the KTH-NASA Wind-Tunnel Model Used for Acquisition of Transonic Nonlinear Aeroelastic Data. AIAA Paper 2017-1814.

[5] Chwalowski, P., Silva, W. A., Wieseman, C. D., et al. (2018). CFD Model of the Transonic Dynamics Tunnel with Applications. NATO AVT-284.

[6] Ivanco, T. G., Keller, D. F., Pinkerton, J. L., et al. (2018). Development of an Atmospheric-Boundary-Layer Profile at the NASA Langley Transonic Dynamics Tunnel. AIAA Paper 2018-5184.

[7] Irwin, H. P. A. H. The Design of Spires for Wind Simulation. *Journal of Wind Engineering and Industrial Aerodynamics*. Elsevier, Vol.7, 1981, pp362-366.

[8] Nayani, S. N., Sellers, W. L., Brynildsen, S. E., et al. (2015). Numerical Study of the High-Speed Leg of a Wind Tunnel. AIAA Paper 2015-2022.

[9] Pirzadeh, S. Z. Advanced Unstructured Grid Generation for Complex Aerodynamic Applications. AIAA Paper 2008-7178.

[10] Samareh, J. A. Unstructured Grids on NURBS Surfaces. AIAA Paper 1993-3454.

[11] NASA LaRC, Hampton, VA (2017). *FUN3D Manual, v13.2*. http://fun3d.larc.nasa.gov.

[12] Roe, P. L. Approximate Riemann Solvers, Parameter Vectors, and Difference Schemes. *Journal of Computational Physics*. Vol. 43, No. 2, 1981.

[13] Spalart, P. R. and Allmaras, S. R. A One-Equation Turbulence Model for Aerodynamic Flows. *La Recherche Aerospatiale*, No. 1, 1994, pp 5–21.

[14] Vatsa, V. N. and Lockard, D. P. (2010). Assessment of Hybrid RANS/LES Turbulence Models for Aeroacoustics Applications. AIAA Paper 2010-4001.

[15] Vatsa, V. N., Carpenter, M. H., and Lockard, D. P. (2010). Re-evaluation of an Optimized Second Order Backward Difference (BDF2OPT) Scheme for Unsteady Flow Applications. AIAA Paper 2010-122.

[16] http://www.mathworks.com/products/matlab/. The MathWorks, Inc. Natick, Massachusetts, USA.

[17] Hobson-Dupont, M. The Development of a Small Scale Wind Tunnel Simulating the Atmospheric Boundary Layer. Master's Theses, San Jose State University, Spring 2015.

## COPYRIGHT STATEMENT